D15

N79-24016

NUMERICAL CALCULATIONS OF HIGH-ALTITUDE DIFFERENTIAL CHARGING:*

PRELIMINARY RESULTS

J.G. Laframboise, R. Godard and S.M.L. Prokopenko
Physics Department, York University

ABSTRACT

A two-dimensional simulation program has been constructed in order to obtain theoretical predictions of floating potential distributions on geostationary spacecraft. The geometry used is infinite-cylindrical with angle dependence. Effects of finite spacecraft length on sheath potential profiles can be included in an approximate way. The program can treat either steady-state conditions or slowly time-varying situations involving external time scales much larger than particle transit times. Approximate, locally dependent expressions are used to provide space-charge density profiles, but numerical orbit-following is used to calculate surface currents. Ambient velocity distributions are assumed to be isotropic, beam-like, or some superposition of these. Preliminary results are presented which demonstrate the readiness of the program to play a useful role in spacecraft charging studies.

INTRODUCTION

A numerical simulation program has been constructed having the following features:
(1) infinite circular cylindrical geometry with angle-dependence
(2) floating surface potential distribution found using "quasistatic iteration" (Laframboise and Prokopenko, 1977) in which sheath potential changes during particle transit times are ignored
(3) calculation of all incident currents by numerical orbit-following, including iterative determination of velocity-space cutoff boundaries for all particle species
(4) use of simplified charge density expressions, rather than numerical orbit-following, in solving Poisson's equation for sheath potentials
(5) incident particle velocity distributions isotropic or beam-like (monokinetic), or some superposition of these
(6) input formats as flexible as possible with regard to inclusion of
    (a) velocity distributions of incident particles, photoelectrons, secondary electrons, backscattered electrons, and gun emissions
    (b) internal current pathways including surface conductive layers
    (c) surface capacitances.

Detailed rationales for the above features have been given by Laframboise and Prokopenko (1977). Effects of finite spacecraft length on sheath potential

* Work supported by the U.S. Air Force Office of Scientific Research under grant no. AFOSR-76-2962.

profiles can be included in either of two approximate ways which lead to modifications of the two-dimensional Poisson equation to be solved. We include here a brief description of these methods, although neither has been used in obtaining the preliminary results presented in Sec. 2. The first method is derived by pretending that the circular inner boundary of the computation grid, which represents the spacecraft surface, is no longer a cross-section of an infinite cylinder, but rather is a cross-section through the equatorial plane of a prolate spheroid of polar-to-equatorial axis ratio $L \geq 1$. We also assume that the sheath potential is (for some unspecified reason) independent of the latitude coordinate perpendicular to this plane. This leads to a modified Poisson equation of the form

$$\tanh^2 \xi \frac{\partial^2 \chi}{\partial \xi^2} + \tanh \xi \frac{\partial \chi}{\partial \xi} + \frac{\partial^2 \chi}{\partial \theta^2} = \frac{\sinh^2 \xi}{\sinh^2 \xi_s} \left(\frac{R_s}{\lambda_D} \right)^2 (n_e - n_i) \tag{1.1}$$

where $\chi = e\phi/kT_e$, ξ is a radial coordinate in the equatorial plane and is related to nondimensional radius $r = R/R_s$, defined in the same plane, by the relation

$r = (L^2 - 1)^{\frac{1}{2}} \sinh \xi$, $\xi_s = \frac{1}{2} \ell n \left[(L+1)/(L-1) \right]$, θ is angular coordinate in the same plane, R_s is spacecraft radius, λ_D is Debye length, and n_e and n_i are the nondimensional electron and ion densities $N_e/N_{e\infty}$ and $N_i/N_{i\infty}$, where N_∞ is ambient density of either species. Use of Eq. (1.1) in place of the usual polar-coordinate Poisson equation would result in sheath potential profiles which became increasingly steeper as L decreased, thus allowing for approximate estimates of sheath potentials around finite cylinders. The limiting case $L = 1$ would correspond to an assumed spherical geometry without latitude dependence; the limit $L \to \infty$ leads to recovery of infinite cylindrical geometry.

The transformation $s = \ell n \coth \frac{1}{2} \xi$ leads to the alternative form

$$\frac{1}{\cosh^2 \xi} \frac{\partial^2 \chi}{\partial s^2} + \frac{\partial^2 \chi}{\partial \theta^2} = \frac{\sinh^2 \xi}{\sinh^2 \xi_s} \left(\frac{R_s}{\lambda_D} \right)^2 (n_e - n_i) \tag{1.2}$$

which contains no first-order terms. For small ξ, s varies logarithmically with r: for large ξ, s varies as r^{-1}.

The second method is derived by first writing the nondimensional Poisson equation for cylindrical coordinates, which has the form

$$\frac{\partial^2 \chi}{\partial r^2} + \frac{1}{r} \frac{\partial \chi}{\partial r} + \frac{1}{r^2} \frac{\partial^2 \chi}{\partial \theta^2} + \frac{\partial^2 \chi}{\partial z^2} = \left(\frac{R_s}{\lambda_D} \right)^2 (n_e - n_i) \tag{1.3}$$

We then assume that $\chi(r,\theta,z)$ is periodic in z, such that values of χ repeat after nondimensional distance 2ℓ parallel to the z axis. In particular, we assume that $\chi(r,\theta,\pm\ell)$ = some given dependence $\chi_\ell(r,\theta)$, and that $\chi(r,\theta,0) = \chi_0(r,\theta)$ to be found. We further assume that $\partial\chi/\partial z = 0$ at $z = 0$, $z = \pm\ell$, $z = \pm 2\ell$, etc, and that only the lowest Fourier component of the z dependence of χ is present. Then

$$\chi(r,\theta,z) = \tfrac{1}{2}[\chi_0(r,\theta) + \chi_\ell(r,\theta)] + \tfrac{1}{2}[\chi_0(r,\theta) - \chi_\ell(r,\theta)] \cos\left(\frac{\pi z}{\ell} \right) \tag{1.4}$$

and, at $z = 0$, we have

$$\frac{\partial^2 \chi_0}{\partial z^2} = \tfrac{1}{2} \left(\frac{\pi}{\ell} \right)^2 [\chi_\ell(r,\theta) - \chi_0(r,\theta)] \tag{1.5}$$

The Poisson equation for $\chi_0(r,\theta)$ now becomes

$$\frac{\partial^2 \chi_0}{\partial r^2} + \frac{1}{r}\frac{\partial \chi_0}{\partial r} + \frac{1}{r^2}\frac{\partial^2 \chi_0}{\partial \theta^2} - \tfrac{1}{2}\left(\frac{\pi}{\ell}\right)^2 \chi_0 = \left(\frac{R_s}{\lambda_D}\right)^2 (n_e - n_i) - \tfrac{1}{2}\left(\frac{\pi}{\ell}\right)^2 \chi_\ell(r,\theta) \quad (1.6)$$

We see that in this Poisson equation, effects of z-dependence are represented by a homogeneous "Helmholtz" term and a fictitious space charge contribution. The z-dependence incorporated into this equation could represent approximately the effects on sheath potentials of finite spacecraft length and/or features such as conductive circumferential bands. Equations (1.2) and (1.6) are both solvable by standard methods; both are linear. Both contain only two (radius and angle) independent variables.

Other numerical simulations of the high-altitude spacecraft charging problem include those of Katz et al. (1977) for a wide variety of three-dimensional geometries, Parker (1978a) for finite circular cylindrical geometry with azimuthal symmetry, and Parker (1978b) for the three-dimensional disturbed region around a thin rectangular plate. All of these treatments use quasistatic iteration. Among older treatments, that of Soop (1972) is noteworthy because it is two-dimensional and fully time-dependent. The treatments of Schröder (1973), Rothwell et al. (1976), Whipple (1976) and Lafon (1976) involve self-consistent calculations of space charge densities but assume that sheath potentials have radial symmetry. The latter is a serious limitation because of the inherently angle-dependent nature of the problem.

RESULTS AND DISCUSSION

Figures 1 - 3 show equipotential contours surrounding an infinite cylindrical spacecraft surface having two independently floating conductive sectors, the smaller of which is shaded in all three cases, and subtends angles of 90°, 45° and 22½°, respectively. In obtaining these results and also those in Figs. 4 and 5, an eight-level discretization in velocity space has been used for each particle species involved (ambient electrons, ambient ions, photoelectrons, and, in Fig. 5, secondary and backscattered electrons). In Figs. 1 - 6, T_{ph} is assumed photoelectron temperature. The calculation was judged to have converged sufficiently when the magnitude of the total unbalanced current to each sector was < 0.01 times the total current of ambient electrons to the same sector. In Figs. 1 and 5, this criterion is unsatisfied on the larger sector and on both sectors, respectively. The resulting floating surface potentials in Figs. 1 - 5 are accurate to within approximately 50 V or better. A noteworthy feature of Figs. 1 - 3 concerns the dependence of the shaded-sector potential on sector angle. The indicated values of -2956V, -2956V and -2969V respectively, provide an indication that ion collection is orbit-limited for sector angles of 90° and 45°, but orbit-limitation has (just) broken down for a sector angle of 22½°. This result is consistent with a prediction by Prokopenko and Laframboise (1977) that the potential well configuration around a sufficiently small shaded electrically isolated surface element can produce breakdown of orbit-limited ion collection on it, driving its floating potential more negative than otherwise.

Figure 4 shows a situation identical to that of Fig. 3 except that the spacecraft has been rotated counterclockwise by 90°, bringing the smaller sector partly into sunlight. As a result, its potential has risen, as expected. At the same time the larger sector, which now has a smaller proportion of its total area sunlit, has become more negative.

Figure 5 shows a situation identical to that of Fig. 3 except that currents due to electron backscattering and also secondary emission caused by electron impact have been included. In comparison with Fig. 3, both sector potentials have risen substantially because of the inclusion of these currents. A barrier of negative potential is now evident on the sunlit side of the spacecraft (Fahleson, 1970; Prokopenko and Laframboise, 1977). In this case, the shaded-sector potential has been influenced more strongly by breakdown of orbit-limited ion collection than in Fig. 3. If such breakdown had not occurred, the shaded-sector potential would have been -1985V. The omission of secondary emission due to ion impact in this calculation causes the floating potentials shown to be slightly more negative than would otherwise be the case.

Figure 6 differs from Figs. 1 - 5 in that the situation shown is for an insulating spacecraft surface, for which a floating condition requires local current balance to exist at every point. It also differs in being not a converged result, but a "guess field" (first-iterate) potential distribution based on a local current balance calculation in which attracted-species currents were assumed orbit-limited everywhere, and all emitted photoelectrons were assumed to escape. The latter assumption is clearly wrong in view of the barrier of negative potential which exists on the sunlit side of the spacecraft. Excess electron collection will therefore occur on sunlit surfaces, driving their potentials more negative. Attempts to converge onto a floating condition have provided qualitative confirmation of such behavior, but successful convergence had not yet been achieved when this was written. The reason appears to involve the fact that on a curved surface, photoemission current decreases continuously as a function of distance from the subsolar point. A point (whose location is not known in advance) will therefore exist at which photoemission becomes insufficient to hold the surface close to space potential. Beyond this point, surface potential will decrease rapidly as a function of position. The surface potential profile will therefore contain a "shoulder" whose location evolves as the calculation proceeds. Combination of this situation with truncation errors in the photocurrent calculation appears to be responsible for the observed lack of convergence. A variety of approaches are presently being explored in an effort to overcome this difficulty, including the construction of a surface-current model for photoemission which includes production-gradient as well as potential-gradient effects.

CONCLUSIONS

We have presented results from a two-dimensional numerical simulation of the high-altitude differential charging problem. Although these results are preliminary, they provide verification of a prediction by Prokopenko and Laframboise (1977) that breakdown of orbit-limited ion collection can occur on a sufficiently small shaded isolated surface element, driving its floating potential more negative than otherwise. The results also verify another prediction (Fahleson, 1973; Prokopenko and Laframboise, 1977) that barriers of negative potential can form on the sunlit side of a differentially charged spacecraft in the absence of space-charge effects. A variety of other phenomena, including effects of time-dependent external conditions, effects of surface material properties including those of "multiple-root" materials (Prokopenko and Laframboise, 1977), and effects of gun emissions remain to be investigated. The results obtained so far provide evidence that the simulation

program is ready to play a useful role in studies of high-altitude spacecraft charging problems.

REFERENCES

Fahleson, U. (1973) Plasma-vehicle interactions in space: some aspects of present knowledge and future development. In: Photon and Particle Interactions with Surfaces in Space, R.J.L. Grard, Editor, D. Reidel Pub. Co., Dordrecht, Holland, pp. 563-569.

Katz, I., Parks, D.E., Wang, S., and Wilson, A. (1977), Dynamic modeling of spacecraft in a collisionless plasma. In: Proc. USAF-NASA Spacecraft Charging Technology Conference, C.P. Pike and R.R. Lovell, Editors, Report No. AFGL-TR-77-0051, Air Force Geophysics Laboratory, Hanscom AFB, Massachusetts/NASA TMX-73537, Lewis Research Center, Cleveland, Ohio, pp. 319-330.

Lafon, J.-P.J. (1976), On the sheath surrounding a conductor emitting photoelectrons in an isotropic collisionless plasma, Radio Sci. 11, pp. 483-493.

Laframboise, J.G., and Prokopenko, S.M.L. (1977), Numerical simulation of spacecraft charging phenomena. In: Proc. USAF-NASA Spacecraft Charging Technology Conference, C.P. Pike and R.R. Lovell, Editors, Report No. AFGL-TR-77-0051, Air Force Geophysics Laboratory, Hanscom AFB, Massachusetts/NASA TMX-73537, Lewis Research Center, Cleveland, Ohio, pp. 309-318.

Laframboise, J.G., and Prokopenko, S.M.L. (1978), Predictions of high-voltage differential charging on geostationary spacecraft, Paper 4.4, 1978 Ionospheric Effects Symposium, Arlington, January 1978 (proceedings in press).

Parker, L.W. (1978), Potential barriers and asymmetric sheaths due to differential charging of nonconducting spacecraft. Report No. AFGL-TR-78-0045, Air Force Geophysics Laboratory, Hanscom AFB, Massachusetts.

Parker, L.W. (1978), Plasma sheath effects on equilibrium voltage distributions of large high-power satellite solar arrays. Paper III-4, 2nd USAF-NASA Spacecraft Charging Technology Conference, Colorado Springs, October 1978.

Prokopenko, S.M.L., and Laframboise, J.G., (1977), Prediction of large negative shaded-side spacecraft potentials. In: Proc. USAF-NASA Spacecraft Charging Technology Conference, C.P.Pike and R.R. Lovell, Editors, Report No. AFGL-TR-77-0051, Air Force Geophysics Laboratory, Hanscom AFB, Massachusetts /NASA TMX-73537, Lewis Research Center, Cleveland, Ohio, pp. 369-387.

Rothwell, P.L., Rubin, A.G., Pavel, A.L., and Katz, L. (1976), Simulation of the plasma sheath surrounding a charged spacecraft. In: Spacecraft Charging by Magnetospheric Plasmas, A. Rosen, Editor, AIAA, New York, and MIT Press, Cambridge, Massachusetts, pp. 121-133.

Schröder, H. (1973), Spherically symmetric model of the photoelectron sheath for moderately large plasma Debye lengths. In: Photon and Particle Interactions with Surfaces in Space, R.J.L. Grard, Editor, D. Reidel Pub. Co., Dordrecht, Holland, pp. 51-58.

Soop, M. (1972), Report on photo-sheath calculations for the satellite GEOS, Planet.Space Sci. 20, pp. 859-870.

Whipple, E.C., Jr. (1976), Theory of the spherically symmetric photoelectron sheath: a thick sheath approximation and comparison with the ATS 6 observation of a potential barrier. J. Geophys. Res. 81, pp. 601-607.

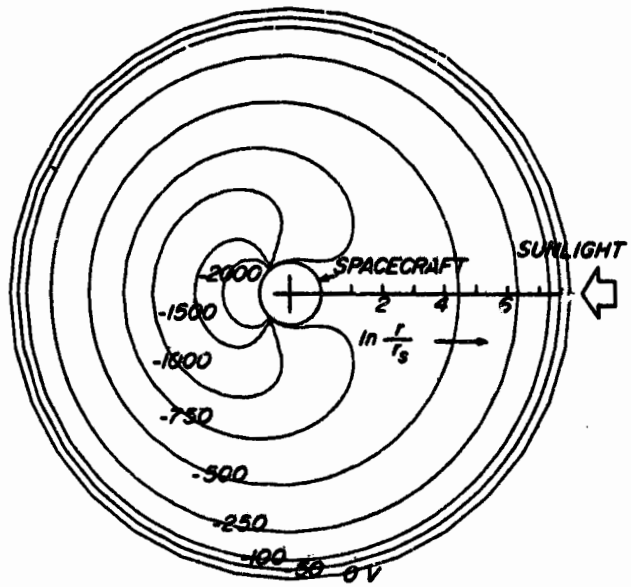

Figure 1. Equipotential contours around an infinite cylindrical spacecraft with two conductive sectors having angles of 270° and 90°. Sector potentials are -735V and -2956V, respectively. Residual sector currents are -0.0066 and -0.0060 times sector electron random currents, respectively. $T_i = T_e =$ 1keV, $T_{ph} =$ 1eV, $N_{e\infty} = 50$ cm^{-3}. Assumed photoemission flux J_{ph} is 42×10^{-6} A/m^2 at normal sunlight incidence (i.e. that for aluminum). Secondary and backscattered fluxes are assumed zero. Computation grid contains 34 x 16 intervals. Space charge is neglected.

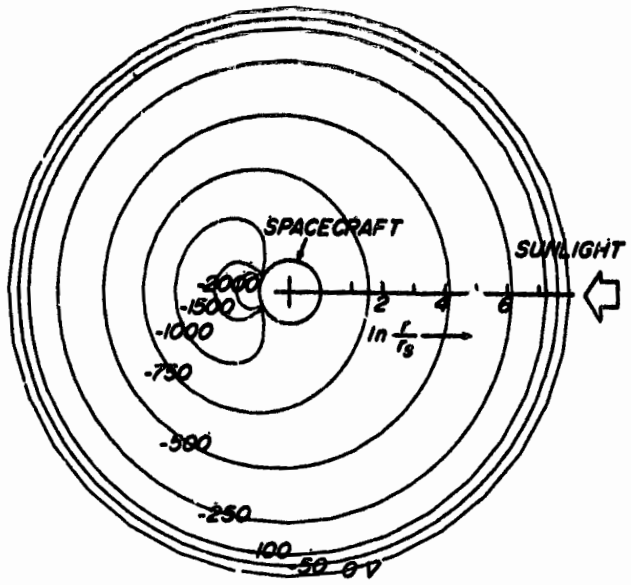

Figure 2. Equipotential contours around an infinite cylindrical spacecraft with two conductive sectors having angles of 315° and 45°. Sector potentials are -856V and -2956V, respectively. Residual sector currents are -0.0038 and -9.0×10^{-7} times sector electron random currents, respectively. Other data are same as for Fig. 1.

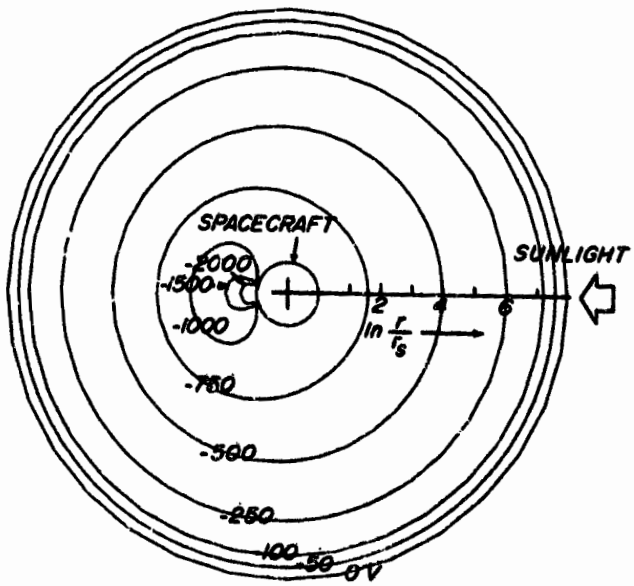

Figure 3. Equipotential contours around an infinite cylindrical spacecraft with two conductive sectors having angles of 337½° and 22½°. Sector potentials are -893V and -2969V, respectively. Residual sector currents are -0.0032 and 2.2×10^{-4} times sector electron random currents, respectively. Other data are same as for Fig. 1.

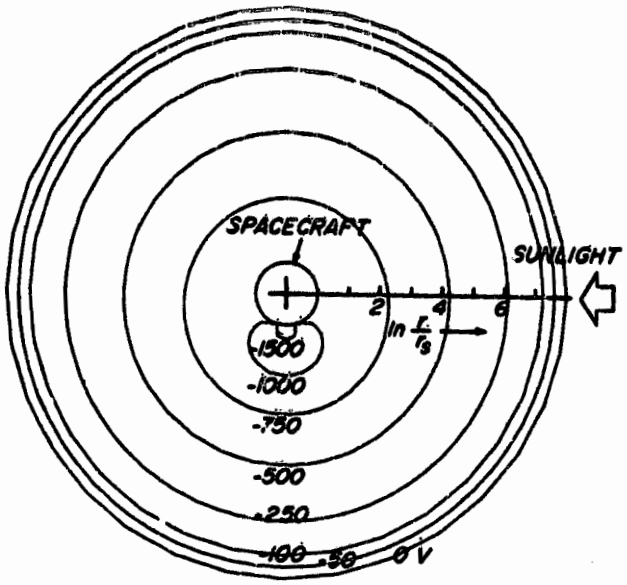

Figure 4. Same as Fig. 3 except rotated by 90° with respect to sunward direction. Sector angles are 337½° and 22½°. Sector potentials are -998V and -1964V, respectively. Residual sector currents are -0.0071 and -7.5×10^{-4} times sector electron random currents, respectively.

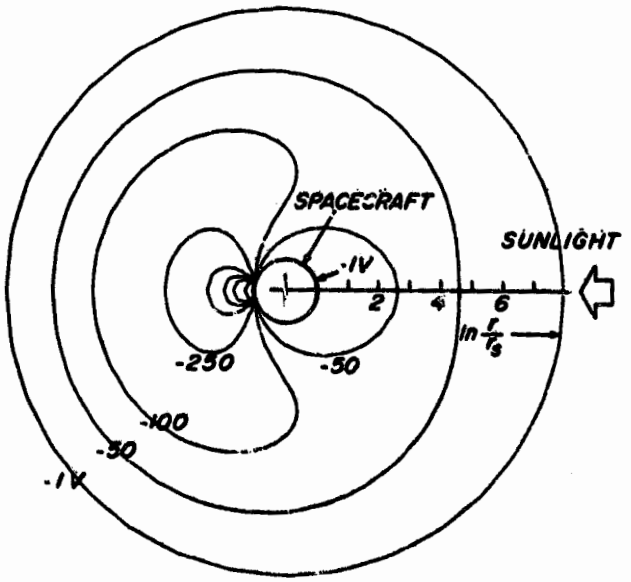

Figure 5. Same as Fig. 3 except that secondary and backscattered currents due to electron impact are included. Sector angles are 337½° and 22½°. Sector potentials are 0.124V and -2126V, respectively. Residual sector currents are -0.042 and 0.021 times sector electron random currents, respectively. Secondary and backscatter data used [illegible] ose given for aluminum by Laframboise and Prokopenko (1978). [illegible] ials on unlabeled contours are -500, -750, -1000, -1500 and -2000V.

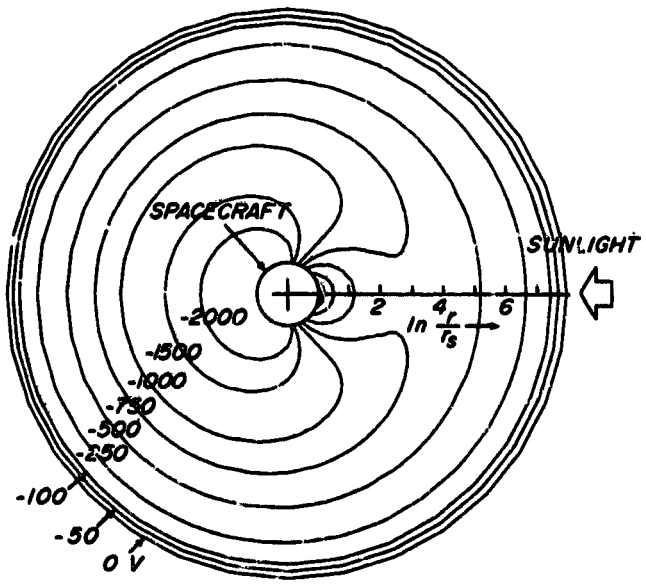

Figure 6. Equipotential contours around an infinite cylindrical spacecraft having an insulating surface, corresponding to a "guess field" surface potential distribution determined using local current balance considerations, with all potential barrier effects ignored. Maximum and minimum surface potentials are 5.42×10^{-3} V and -2956V, respectively. Assumed values of T_i, T_e, $N_{e\infty}$, T_{ph} and J_{ph} are the same as for Fig. 1. Secondary and backscattered fluxes are assumed zero. Computation grid contains 34 x 16 intervals. Space charge is neglected.